processes

MDPI

Article

Research on Managed-Pressure Running Casing in Oil and Gas Wells with the Negative Pressure Window

Yuntao Mei [1,2], Huanqiang Yang [1,2,*], Zhuo Zhang [3] and Mengjia Ji [4]

[1] College of Petroleum Engineering, Yangtze University, Wuhan 430100, China; 2021720411@yangtzeu.edu.cn
[2] National Engineering Research Center for Oil & Gas Drilling and Completion Technology, Yangtze University, Wuhan 430100, China
[3] Engineering Technology Department of Western Drilling Company, Karamay 834000, China
[4] Sinopec Zhongyuan Oilfield, Puyang 457000, China; 202072342@yangtzeu.edu.cn
* Correspondence: yanghuanqiang@yangtzeu.edu.cn

Abstract: The failure of managed-pressure running casing in oil and gas wells may lead to complex accidents such as overflow or leakage. The technique of using multi-density gradient drilling fluids in wellbores with negative pressure windows (NPWs) is often used to deal with this situation. Therefore, it is vital to analyze the dynamic slurry column structure and calculate the wellbore pressure during casing running. For this issue, the model of transient surge pressure is established during casing running. The calculation equation of the model is proposed, and the calculations of the wellbore pressure are carried out with the exploration of Well LT-X1, located in the Xinjiang oil field. A circulation scheme is designed as follows: Circulate 125 m^3 of drilling fluid with a density of 2.45 g/cm^3 and 155 m^3 of drilling fluid with a density of 2.35 g/cm^3 at a depth of 3560 m. From there, circulate 164 m^3 of drilling fluid with a density of 2.35 g/cm^3 at a depth of 5900 m. Finally, at a depth of 7050 m, circulate 250 m^3 of drilling fluid with a density of 2.30 g/cm^3. The casing running speeds and back-pressure values were designed as follows for the respective well sections: 0–1523 m: 0.160 m/s casing speed, 0 MPa back pressure; 1523–3560 m: 0.160 m/s casing speed, 1.641 MPa back pressure; 3560–5900 m: 0.145 m/s casing speed, 2.427 MPa back pressure; 5900–6674 m: 0.137 m/s casing speed, 4.041 MPa back pressure; 6674–7050 m: 0.124 m/s casing speed, 4.457 MPa back pressure. The results show that optimizing structure of the multi-density gradient drilling fluid with different densities and applying annular back pressure in stages, with the accurate calculation of wellbore pressure, can achieve the goals of leak-proofing and pressure-stabilization. It is concluded that this result may serve as the foundation for managed-pressure running casing technology.

Keywords: negative pressure window; managed-pressure running casing; multi-density gradient drilling fluids; transient surge pressure; leak-proof and pressure-stabilized

Citation: Mei, Y.; Yang, H.; Zhang, Z.; Ji, M. Research on Managed-Pressure Running Casing in Oil and Gas Wells with the Negative Pressure Window. *Processes* **2023**, *11*, 2210. https://doi.org/10.3390/pr11072210

Academic Editors: Tianshou Ma and Yuqiang Xu

Received: 26 June 2023
Revised: 16 July 2023
Accepted: 18 July 2023
Published: 22 July 2023

1. Introduction

Complicated formation pressure systems, such as NPWs in oil and gas wells, are increasing, which may lead to complex accidents. Lost circulation and overflow in the wellbore are two typical accidents that occur when the wellbore pressure is beyond the scope of pore pressure and leakage pressure during the drilling operation [1–3]. To solve this problem, managed-pressure drilling (MPD) continues to rely on the back pressure applied by the surface high-pressure pump at the wellhead to precisely control the annular pressure profile, despite the noise pollution generated by the high-pressure pump [4]. After drilling to the predetermined depth with MPD technology, the next step is always to pull out of hole (POOH) and prepare the next construction called casing running. The calculation of wellbore pressure in the processes of pre-casing preparation, down-casing and drilling fluid circulation are important for developing the casing running plan reasonably and adjusting the back pressure in a timely manner.

Surge pressure, generated during the process of casing running, is an important part of wellbore pressure that is crucial for avoiding complex accidents in wellbores. In various working conditions, extensive studies have been conducted to analyze and gain a comprehensive understanding of surge pressure. The field studies aimed to examine the impact of fluid properties and wellbore geometry on surge and swab pressures [5–9]. The findings of these studies consistently indicate that both surge pressures exhibit a positive correlation with increasing tripping speeds and wellbore depths. These studies only investigated two types of surge pressures, both of which are positively correlated with an increase in tripping speeds and wellbore depths. More recent studies have further confirmed the strong impact of tripping speeds, wellbore geometry, flow regime, and fluid rheology on surge pressures [10–16].

However, the drilling industry greatly relies on surge models and simulators. At present, some models, including steady-state models and transient models, have been proposed to calculate the surge pressure during POOH and casing running processes. Before the 1970s, the models were mainly based on the theory of the steady-state method and usually considered the fluid in the wellbore as a Newtonian model [17–20]. Furthermore, more and more models were developed considering the Bingham model, power-law model and Roberston–Stiff model [21–23]. In recent years, the impact of stabilizer placement on the annular clearance has been taken into account in the prediction of the volatility stress model [24]. Meanwhile, the error of surge pressure calculation results reaches ±3% [25]. These models mainly analyze the influence of drilling fluid density, stabilizer quantity, annular clearance, and drill string eccentricity on the surge pressure. In summary, while surge models and simulators have made significant progress in predicting surge pressure during POOH and casing running processes, there are limitations in capturing the full complexity of fluid behavior and accurately accounting for all factors that influence surge pressure. Further research and advancements are needed to improve the accuracy and reliability of surge models in the drilling industry.

After mid-1970s, with the improvement of computer calculation capabilities, the transient method was applied in the calculation of surge pressure. Fluid compressibility, duct wall expansion, and fluid inertia were considered with the establishment of the surge pressure model [26]. The variation of maximum surge pressure and swabbing pressure at each depth within the wellbore with time were predicted proposed solving the transient surge pressure of each passage using the mixing implicit feature line method, which obtained the numerical solutions of transient surge pressure under various conditions [27]. To acquire the wellbore pressure and ground stress field in the near-wellbore section of deep-water drilling, some scholars proposed a method for analyzing wellbore stability based on the oscillation coupling of transient surge pressure [28]. Considering the liquid–solid two-phase medium, researchers studied the transient surge pressure during tripping operations with the use of the numerical simulation method [29]. Based on the transient method, the effect of overflow, drilling speed and acceleration were analyzed in the calculation of surge pressure [30,31]. Using spectrum analyses, it was found that high-pressure hoses are most susceptible at certain frequencies to deformation, and to the response and surge pressures of the fluid within. This can even lead to irreversible degradation changes in the internal structure of the hose [32]. However, it is important to note that despite the advancements and insights gained from these studies, there are limitations to consider. The basis of their model establishment is limited to a single-density fluid within the wellbore.

The above-established calculation models for the surge pressure are all based on homogeneous fluid within the wellbore and cannot be applied to drilling fluids with multiple density gradients that are usually used in wells with NPW. This paper presents the structure of the slurry column and surge pressure calculation models during the casing running process, considering the drilling fluids with multiple density gradients in the wellbore. Taking Well LT-X1 as an example, the pressure-managed technology for casing running under NPWs is developed.

The formation pressure data of Well LT-X1 are shown in Figure 1. At the depth of 5852 m, and 6152 m in the wellbore, the equivalent densities of pore pressure and leakage pressure are 2.49 g/cm^3 and 2.52 g/cm^3, 2.425 g/cm^3 and 2.445 g/cm^3, respectively. The leakage pressure at the depth of 6152 m is lower than the pore pressure at 5852 m, which is defined as the NPW. So, the reservoir pore pressure cannot be balanced by drilling fluid for which the density is equal to pore pressure. This will result in lost circulation at the bottom of the hole and kick (probably evolving to blowout) at the upper depth of the well. MPD technology was employed in this well at the key well sections with NPWs. After drilling, the drill rods are pulled out of hole, and the fluid in the wellbore will have a loss of circulation. Therefore, drilling fluids with multi-density gradient column structures are needed to balance the reservoir pore pressure.

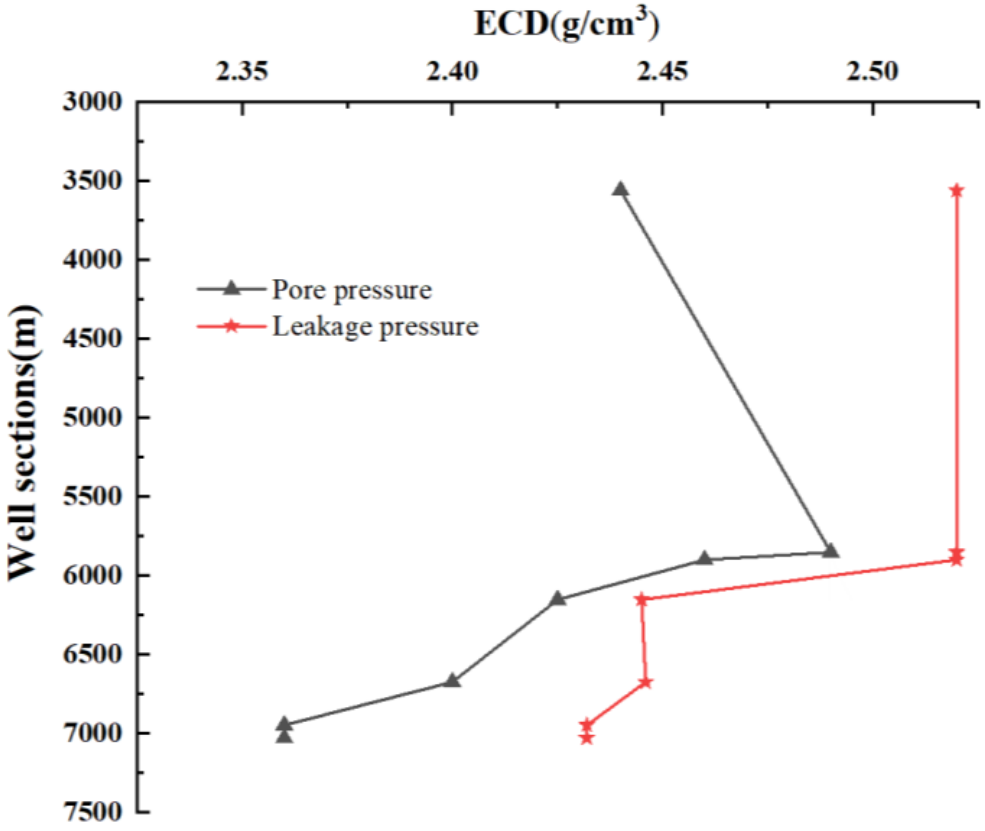

Figure 1. The formation pressure of Well LT-X1 with an NPW.

2. Methodology

2.1. Model Description

As shown in Figure 2a, we assume there is an oil and gas well drilled to a depth of H, which has n sets of pressure systems with the depths of H_1', H_2', H_3', ... , H_n' in an open-hole section, and the corresponding pore pressure and leakage pressure are (ρ_{p1}, ρ_{f1}), (ρ_{p2}, ρ_{f2}), (ρ_{p3}, ρ_{f3}), ... , (ρ_{pn}, ρ_{fn}), respectively. The density of drilling fluid in the wellbore is ρ_0, since the leakage pressure ρ_{f1} at the bottom hole is less than the pore pressure at the upper depth, and the design method of slurry column structures with multi-density gradients is adopted as follows.

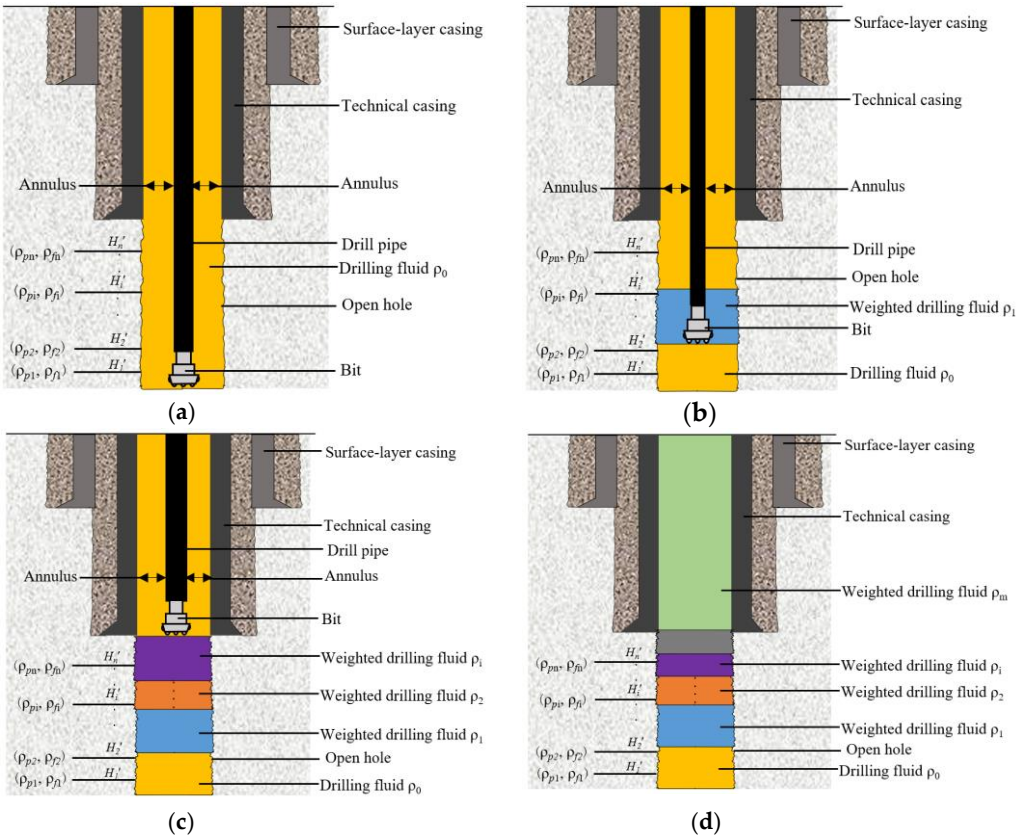

Figure 2. Slurry column structure in the wellbore during tripping. Each drilling fluid density ρ_i and length h_i are designed with the requirements of the formula (**a**) Before tripping; (**b**) Drilling fluid circulation after tripping; (**c**) Drill to a certain height; (**d**) Drilling completed.

(1) To stabilize the upper formation and prevent leakage, a substitution is made by replacing a portion of the bottom-hole drilling fluid ρ_0 with weighted drilling fluid ρ_1 before commencing the tripping-out process.

(2) After raising the drill pipe string to a specific height, the height of the weighted drilling fluid ρ_1 is changed to h_1. This adjustment is necessary to stabilize the upper formation and facilitate the circulation of the weighted drilling fluid ρ_2, as shown in Figure 2b.

(3) The design of the height h_i of the tripped-out drill pipe string and the density of the weighted drilling fluid ρ_i is based on the specific pressure systems involved, as shown in Figure 2c.

(4) The hydrostatic column pressure of the multi-density gradient drilling fluid in the wellbore plays contributes entirely to preventing leaks and ensuring pressure-stabilization after all the drill pipe strings are pulled out The density ρ_i and length h_i of the multi-density gradient drilling fluids are designed as (ρ_1, h_1), (ρ_2, h_2), (ρ_3, h_3), ... , (ρ_m, h_m), respectively, as shown in Figure 2d.

$$\rho_{oj} \leq \sum_{j=k}^{m} \rho_i g h_i \leq \rho_{pj} \quad (1)$$

2.2. Model of Slurry Column Structure

In the construction process of this well, step-by-step casing running is employed, accompanied by the circulation of drilling fluids with different densities. Typically, the pipe string, comprising the casing string and the drill pipe string, is run into the well during the casing running procedure, as depicted in Figure 3. As the drilling pipe string is inserted, the

fluid volume in the well is continuously drained by the pipe string. Furthermore, once the casing string reaches a certain depth, the drilling fluids in the well must be circulated and discharged using another drilling fluid from the wellhead. Calculating the slurry column structure in the wellbore during casing running poses particular challenges, especially in oil and gas wells with complex wellbore structures. In order to accurately calculate the slurry column structure in the wellbore during casing running, the following calculation methods are established.

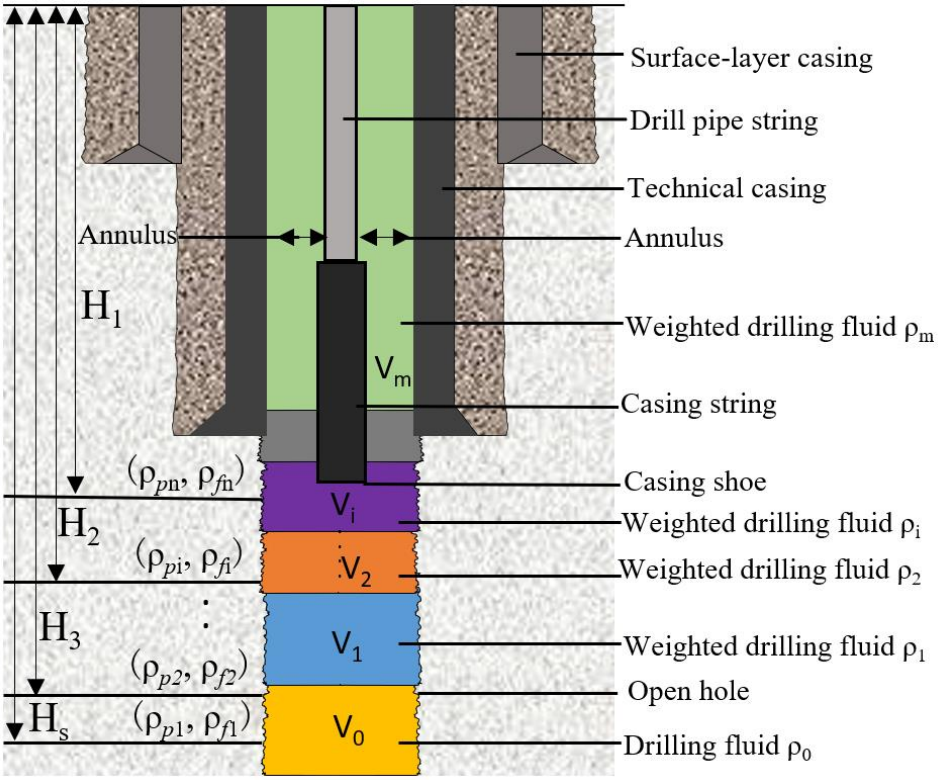

Figure 3. Casing running process diagram.

(1) Assume that the volumes of multi-density gradient drilling fluids in the wellbore from bottom to top are V_0, V_1, V_2, ... , V_m, respectively. The lengths of the drill pipe string and the production casing used for cementing are denoted as *LD* and *LC*, respectively. The total well depth is given by the sum of LD and LC. The casing running process is divided into s stages, the casing running speeds in each stage are denoted as v_1, v_2, v_3, ... , v_s, respectively, and the corresponding well running depths are H_1, H_2, H_3, ... , H_s, respectively, as shown in Figure 3.

(2) Calculate the volume *Vp* of the drill pipe string and production casing in the well at any time and compare it with the sum of the volume V_f of the first *k* fluids (from top to bottom) in the wellbore, as shown in Equation (2). If $V_p > V_f$, the m, $m-1$, $m-2$, ... , k fluids will be replaced out of the wellbore; otherwise, $k = k-1$, and repeat step (2).

$$V_f = \sum_{i=k}^{m} V_i \quad (2)$$

(3) The calculation process of the fluid slurry column structure in the annulus above the casing shoe is complex; it is shown in Figure 4.

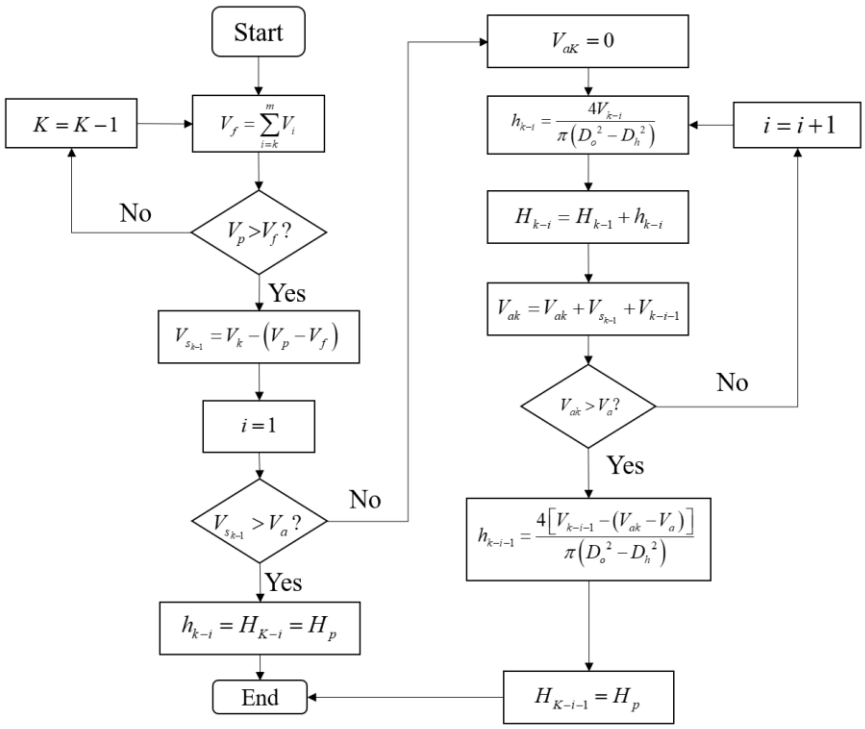

Figure 4. Calculation flow chart of annular fluid slurry column structure during the casing running process.

where V_{Sk-1} is the $k-1$ residual fluid volume in the wellbore, m^3; V_a is the volume of the annulus above the casing shoe, m^3; h_{k-1} is the height of $k-1$ fluid in the annulus, m; H_{k-1} is the top depth of $k-1$ fluid, m; V_{ak} is the sum of the volumes of $k-i-1$ fluids in the annulus, m^3; D_o is the outer diameter of the annulus, m; and D_h is the inner diameter of the annulus, m.

(4) When casing is run into the well, it reaches a depth of Hp in the p stage. At this stage, drilling fluid with a density of ρ_{cp} is injected from the drill pipe string at the wellhead, filling both the drill pipe string and the annular space. Subsequently, casing continues to be run to a depth of H_{p+1} in the $p = p + 1$ stage, and the process described in Equation (2) to (3) is repeated to calculate the slurry column structure in the wellbore during the casing running process.

The calculation of the wellbore fluid column pressure P_h when running casing to the depth of H_p can be formulated as:

$$P_h(H_p) = \sum_{n=0}^{k-i} \rho_n g h_n + \sum_{j=k-i}^{k-1} \rho_j g H_j \quad (3)$$

where ρ_n is the density of the drilling fluid in the n-section of the upper annular space of the casing shoe, g/cm^3; H_n is the length of the drilling fluid column of the n-section of the annular space, m; ρ_j is the density of drilling fluid in the lower j-section of the casing shoe, g/cm^3; and H_j is the length of the drilling fluid column in the lower j-section of the casing shoe, m.

In situations where the drill pipe string does not fully enter the well, the ground equipment is unable to control the annular pressure. The wellbore pressure under such circumstances is the combination of the hydrostatic column pressure P_h and the surge pressure Po. The wellbore pressure P_1 during casing running up to the depth of Hp can be formulated as:

$$P_1 = P_o(v_p) + P_h(H_p) \quad (4)$$

With the complete insertion of the drill pipe string into the well, back pressure can be applied to stabilize the formation. The wellbore pressure during this phase comprises three key elements: the hydrostatic column pressure P_h at the lower and upper ends of the casing shoe, the surge pressure *Po* induced by casing running, and the back pressure P_b exerted by ground equipment.

The wellbore pressure $P_1{}'$ during casing running to the depth of H_p can be formulated as:

$$P_1{}' = P_0(v_p) + P_h(H_p) + P_b \tag{5}$$

The algorithm of this model has been implemented in Visual Studio platform using the C# programming language to calculate the mid-column structure in the wellbore during the casing running process.

2.3. Model of Wellbore Pressure

During the casing running operation, the wellbore is divided into two parts: *LD* (above the casing shoe) and *LC* (below the casing shoe). This division allows for the analysis and calculation of the wellbore pressure. Furthermore, considering the specific working conditions of casing running operations, two stages of wellbore pressure-control models are developed. These models are utilized to calculate the wellbore pressure during both the casing running process and the circulating drilling fluid process.

2.3.1. Wellbore Pressure during Casing Running

When the DP non-completely enters into the well, the annular pressure cannot be managed by the ground equipment. The wellbore pressure at this time is P_1. The speed of the lower casing within the safe density window range in this formation can be calculated using the following formula:

$$P_1 = P_0(v_p) + P_h(H_p) < P_{Leakage} \tag{6}$$

When the DP completely enters into the well, back pressure can be applied to stabilize the formation. In this case, the wellbore pressure at this time is $P_1{}'$. Strict control of the wellbore pressure within the safe density window is required to ensure the safe lowering of the pressure control equipment into the well. The model analysis diagram is shown in Figure 5.

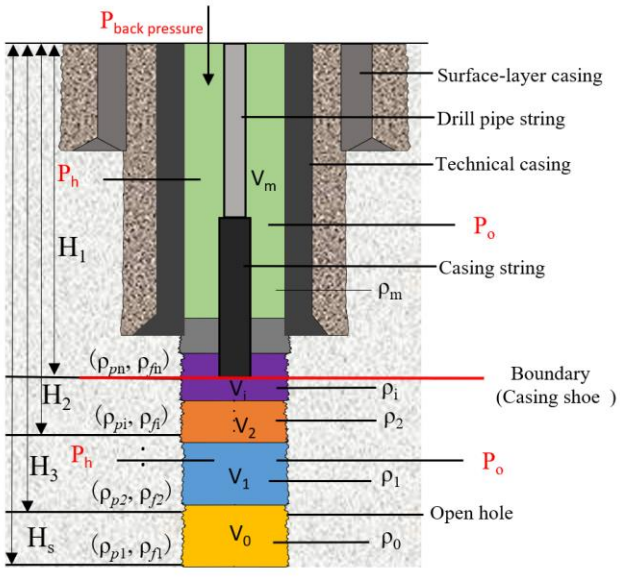

Figure 5. Schematic diagram of wellbore pressure model analysis during casing running.

And the wellbore pressure calculation model is formulated as:

$$P_1\prime = P_0(v_p) + P_h(H_p) + P_b < P_{Leakage} \tag{7}$$

By performing calculations of the hydrostatic column pressure and surge pressure, the correlation between wellbore pressure and casing running speed can be established. This analysis facilitates the determination of the appropriate casing running speed and back-pressure compensation values within the safe density window range.

2.3.2. Surge Pressure

In Formulas (4) and (5), the surge pressure $P_o(v_p)$ plays a crucial role in calculating the wellbore pressure. To account for the pressure changes transmitted to the wellhead and bottom hole, the calculations of surge pressure utilize the transient-flow method based on unstable flow theory.

The normal pressure window casing assumes the presence of a single drilling fluid in the wellbore. However, under the normal pressure window (NPW), there are multiple types of drilling fluids present in the casing wellbore, making the calculation of the friction pressure drop more complex. An accurate calculation of friction pressure drop is crucial for modeling surge pressure. The model of the slurry column structure is based on the principles described in Section 2.2, and the friction pressure drop in the annular space is formulated as:

$$P_f = \sum_{j=k-i}^{k-1} \frac{4K_jH_j}{D_{hy}}\left(\frac{2n_j+1}{3n_j}\frac{12v}{D_{hy}}\right)^n \tag{8}$$

where K_j *is* the consistency coefficient of the jth fluid, Pa·s^n; H_j is the return distance of the jth fluid, m; n is the liquidity index of the jth fluid; and D_{hy} is the hydraulic diameter of the annular space, m.

(1) Governing Equation

Based on the principles of mass and momentum conservation, the governing equation for one-dimensional unstable flow in the wellbore can be derived as follows (9) and (10):

$$\begin{cases} v\frac{\partial p_0}{\partial z} + \frac{\partial p_0}{\partial t} + \rho C^2\frac{\partial v}{\partial z} = 0 \\ \frac{\partial p_0}{\partial z} + \rho\frac{\partial v}{\partial t} + \rho v\frac{\partial v}{\partial z} + p_f = 0 \end{cases} \tag{9}$$

where

$$C = \frac{1}{\sqrt{\rho(\alpha+\beta)}} \tag{10}$$

where Q is the flow rate of drilling fluid, L/s; p is the surge pressure, MPa; C is the propagation velocity of the pressure wave, m/s; A is the cross-sectional area of flow channel, m^2; t is the casing decentralization time, s; Z is the ordinate value along casing, m; p_f is the friction pressure drop, MPa; β is the expansion coefficient of the flow channel; α is the compression coefficient of drilling fluid; and ρ is the density of drilling fluid, g/cm^3.

(2) Grid Division

The characteristic curve method is employed to solve the system of governing equations. Firstly, the characteristic equation of the governing equations (Equation (9)) is established using the modified Lister method. Subsequently, the finite difference method is applied to solve the characteristic equation, yielding the solution for the governing equations.

The characteristic equation of governing equationsis formulated as Formula (11).

$$\begin{cases} \pm dp_0 + \rho C dv + Cp_f dt = 0 \\ \frac{dz}{dt} = v \pm C \end{cases} \tag{11}$$

The forward characteristic line, originating from point M with a slope of arctan ($\frac{1}{v+c}$) intersects the backward characteristic line, originating from point N with a slope of arctan ($\frac{1}{v-c}$), at point T. In the case where the selected Δz and Δt are sufficiently small, the short line segments of the characteristic lines MT and NT can be approximated as straight lines, as shown in Figure 6.

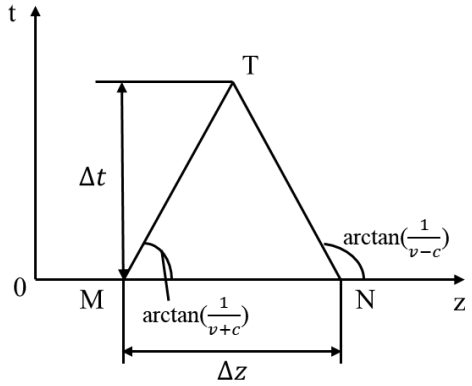

Figure 6. Characteristic diagram.

On the lines MT and NT, the system of equations can be satisfied:

$$\begin{cases} dp_0 + \rho C dv + C p_f dt = 0 \\ -dp_0 + \rho C dv + C p_f dt = 0 \end{cases} \tag{12}$$

The finite difference representation of Equation (12) can be expressed as follows:

$$\begin{cases} p_T - p_M + \rho C(v_T - v_M) + C\Delta t p_{fM} = 0 \\ -p_T + p_N + \rho C(v_T - v_N) + C\Delta t p_{fN} = 0 \end{cases} \tag{13}$$

If P_M, Q_M, P_{fM}, P_N, Q_N, P_{fN} are known, Q_T, P_T can be obtained as follows:

$$Q_T = \frac{p_M - p_N + v(v_M + v_N) - C\Delta t(p_{fM} + p_{fN})}{2\rho C} \tag{14}$$

$$P_T = \frac{p_M + p_N - \rho C(v_M - v_N) - C\Delta t(p_{fM} - p_{fN})}{2} \tag{15}$$

The instantaneous pressure P_T and flow Q_T at any point in the flow channel at any time are obtained.

(3) Boundary Conditions

During actual casing operations, the movement of the casing string within the wellbore induces fluid motion, which can be divided into two distinct flow paths: the annular flow path above the casing shoe and the open-hole flow path below the casing shoe. The surge pressure, resulting from the casing string movement, originates at the casing shoe and gradually attenuates towards both the wellbore and the bottom of the well. The wellhead boundary of the annular flow path is connected to the atmosphere, thereby maintaining a pressure of 0 MPa. At the junction point, which corresponds to the casing shoe, the pressures of both flow paths are equal. The fluid at the casing shoe is displaced by the casing string, causing the fluid within the annular flow path to ascend, while the fluid within the open-hole flow path at the well's bottom descends. Neglecting the permeation of drilling fluid at the well's bottom, the flow rate at the bottom boundary of the open-hole flow path is 0. The sum of the flow rates at the junction point, i.e., the casing shoe, equals the flow rate of casing string displacement. The junction point diagram is shown in Figure 7:

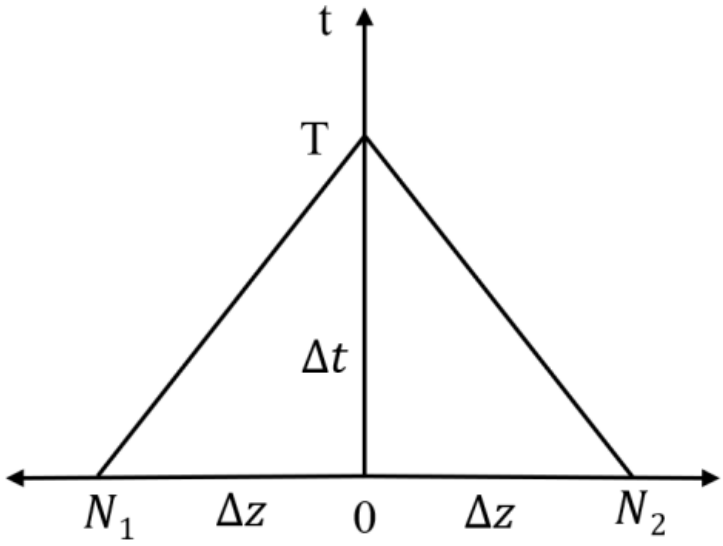

Figure 7. Junction point diagram.

a. The pressure at the wellhead boundary of the annular channel is 0, and the flow rate can be calculated using the equations of the forward characteristic line:

$$\begin{cases} p_T = 0 \\ Q_T = \frac{p_M + \rho C_M v_M - C_M \Delta t p_{fM}}{\rho v_M} \end{cases} \tag{16}$$

b. The flow rate at the bottom-hole boundary of the bottom-hole channel is 0, and the pressure can be determined using the equations of the forward characteristic line.

$$\begin{cases} Q_T = 0 \\ p_T = p_M + \frac{\rho C_M}{A_M} Q_M - C_M \Delta t p_{fM} \end{cases} \tag{17}$$

c. The displacement flow at the junction point, i.e., the casing shoe, is equal to the sum of the flow rates in the two channels. The equations be expressed as follows:

$$\begin{cases} Q_P = Q_{T1} + Q_{T2} \\ p_T = p_{N1} + \frac{\rho C_{N1}}{A_{N1}} (Q_{T1} - Q_{N1}) + C_{N1} \Delta t p_{fN1} \\ p_T = p_{N2} + \frac{\rho C_{N2}}{A_{N2}} (Q_{T2} - Q_{N2}) + C_{N2} \Delta t p_{fN2} \end{cases} \tag{18}$$

By combining Equations (14) and (15), the pressure and flow rate at each position in the wellbore during the casing running process can be obtained by substituting the fixed-solution conditions.

2.3.3. Wellbore Pressure during Drilling Fluid Circulation

During the drilling fluid circulation process, the drilling fluid is injected from the casing and returns through the annular space. The wellbore pressure P_2 during this process consists of the hydrostatic column pressure and the friction pressure drop P_f of the drilling fluids in the annular space with varying densities. The model analysis diagram is shown in Figure 8:

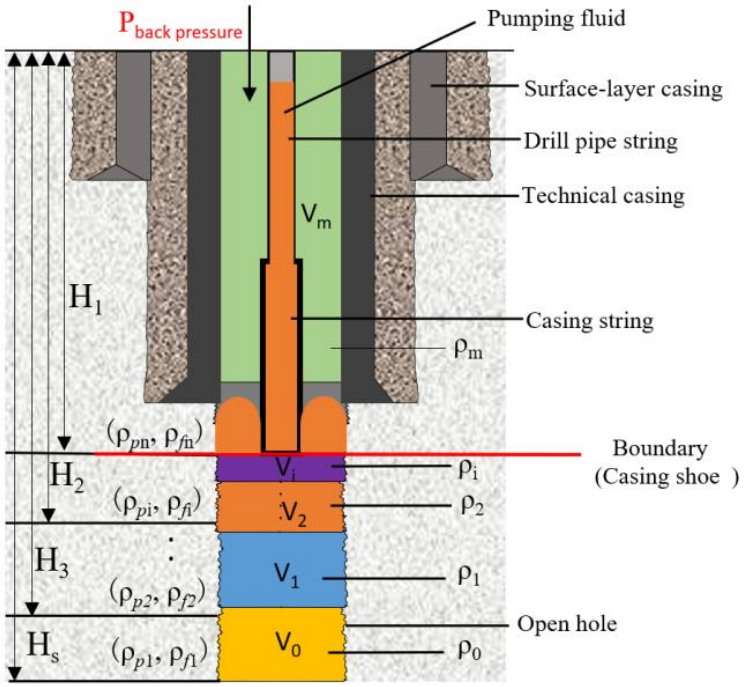

Figure 8. Schematic diagram of wellbore pressure model analysis in the process of circulating drilling fluid.

The formula for calculating the wellbore pressure during the circulating drilling fluid process is expressed as:

$$P_2 = P_h(H_p) + P_f < P_{Leakage} \tag{19}$$

Taking the drilling fluid as a power-law fluid, the friction pressure drop in the annular space is formulated as:

$$P_f = \sum_{j=k-i}^{k-1} \frac{4K_j H_j}{D_{hy}} \left(\frac{2n_j + 1}{3n_j} \frac{12v}{D_{hy}}\right)^n \tag{20}$$

where K_j *is* the consistency coefficient of the jth fluid, Pa·s^n; H_j is the return distance of the jth fluid, m; n is the liquidity index of the jth fluid; D_h is the diameter of the annular space, m; D_{co} is the casing diameter, m; v is the mean flow rate, m/s; D_{hy} is the hydraulic diameter of the annular space, m; and Q is the displacement, L/s.

The mean flow rate is formulated as:

$$v = \frac{4Q}{\pi(D_h^2 - D_{co}^2)} \tag{21}$$

3. Case Study

Well LT-X1 is an exploratory well located in the Xinjiang oil field, situated in the thrust belt of the Homatu anticline and Tugulu anticline in the southern margin of the Junggar Basin. The total depth of the well is 7050 m. To validate the reliability of the model established in this study, a case analysis is conducted on Well LT-X1. The formation pressure of the five layers starting from 5610 m in the open hole of this well is shown in Table 1. The last column of data is the density of drilling fluid circulating during the practical drilling process.

Table 1. Formation pressure of open-hole layers in Well LT-X1.

Serial Number	Well Section (m)	Layer	Pressure Coefficient	Drilling Fluid Density (g/cm^3)
				Practical
1	5610–5745	/K1h	2.54–2.49	2.39–2.41
2	5745–6012	/K1h-K1q	2.48–2.45	2.34–2.40
3	6012–6158	K1q	2.45–2.42	2.55–2.59
4	6158–6806	K1q	2.42–2.40	2.56–2.57
5	6806–7050	J3k	2.39–2.34	2.34–2.36

The MPD data indicated that the well had four leaky layers, with equivalent cycle densities (ECD) at depths of 6152 m, 6674 m, 6947 m and 7028 m of 2.445 g/cm^3, 2.446 g/cm^3, 2.432 g/cm^3 and 2.432 g/cm^3. It can be seen that the formation pressure of section 5610–5745 m and section 5745–6012 m is greater than the leakage pressure of 6672–6674 m, 6946–6947 m and 7026–7028 m, which are typical of NPW wells. The pressure system is complex, posing challenges in determining the casing running speed. By simulating the wellbore's slurry column structure and the variation in wellbore pressure during casing running, a drilling fluid circulation scheme is developed for the casing running process, along with recommended casing velocities and pressure control values for different stages.

3.1. The Slurry Column Structure Inside the Wellbore after Drilling

Combined with the design model of the wellbore slurry column structure and the formation pressure system of each layer in the open hole of Well LT-X1, Table 2 shows the designed slurry column structure.

Table 2. Slurry column structure in wellbore after managed-pressure tripping.

Well Depth Position (m)	Length(m)	Density (g/cm^3)	Fluid Column Pressure (MPa)	Equivalent Density (g/cm^3)
1521	1521	2.50	37.352	2.500
3558	2037	2.50	49.957	2.500
5850	2292	2.38	53.513	2.453
5900	50	2.38	1.121	2.452
6150	250	2.35	5.809	2.448
6300	150	2.35	3.412	2.446
6672	372	2.10	7.705	2.427
6946	274	2.10	5.624	2.414
7026	80	2.10	1.669	2.410
7050	24	2.10	0.453	2.409

3.2. Casing Running Speed

When the casing is being run to a certain depth, drilling fluid circulation is required. Three different density-gradient drilling fluid circulation schemes were designed based on the calculation method of the slurry column structure in the wellbore during the casing running process and in combination with the formation pressure system, as shown in Table 3.

Table 3. Circulating drilling fluid scheme at different depths of casing running.

Casing Depth (m)	Scheme 1	Scheme 2	Scheme 3
3550	2.43 g/cm^3 + 2.32 g/cm^3	2.45 g/cm^3 + 2.35 g/cm^3	2.47 g/cm^3 + 2.38 g/cm^3
5900	2.32 g/cm^3	2.35 g/cm^3	2.38 g/cm^3
7050	2.32 g/cm^3	2.30 g/cm^3	2.28 g/cm^3

The wellbore pressure is calculated using the model described in Section 2.3.3 for the three proposed schemes, as illustrated in Figure 9. In scheme 1, the equivalent circulating density (ECD) in the section from 6500 to 7100 m exceeded the ECD of the leakage layers. In scheme 3, the ECD in the section from 5900 to 6600 m exceeded the leakage ECD. Scheme 2 had an ECD within the safe density window range, and thus the drilling fluid circulation plan for scheme 2 is selected.

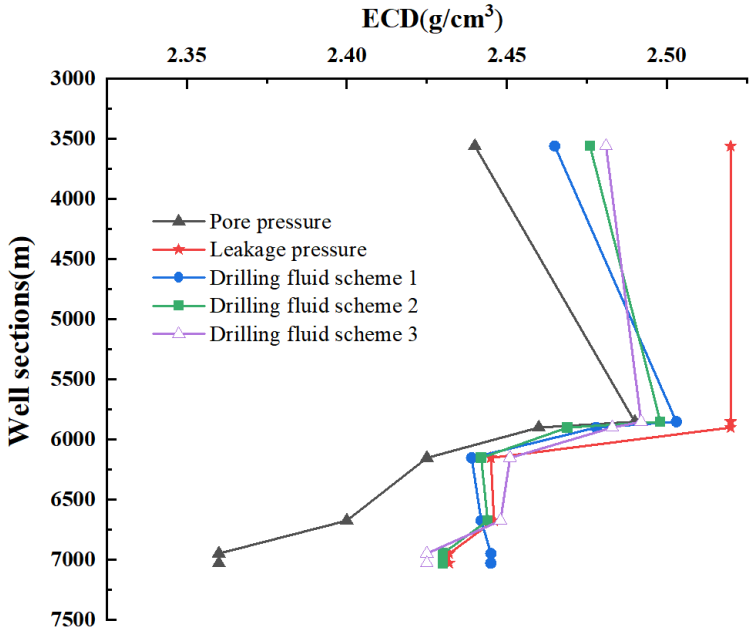

Figure 9. Changes of ECD under different circulating drilling fluid schemes.

Based on the formation pressure system, the density and volume of the circulating drilling fluid for scheme 2 can be calculated. Additionally, the corresponding annular back pressure P_b required during the circulation process is determined. The calculated values are summarized in Table 4:

Table 4. Circulation drilling fluid density when running casing into different positions.

Casing Depth (m)	Circulating Drilling Fluid Density (g/cm^3)	Volume (m^3)	Pressure Control Values (MPa)
3560	2.45	125	0.40–0.10
	2.35	155	1–4.6
5900	2.35	35	4.65
		45	3.90
		40	3.27
		44	2.64
7050	2.30	250	3.60–6.40

According to the calculation model of wellbore pressure during casing running, three schemes of casing speed were designed, as shown in Table 5.

Table 5. Casing speed scheme for casing into different well depth sections.

Casing into the Well Depth Section (m)	Scheme 1 (m/s)	Scheme 2 (m/s)	Scheme 3 (m/s)
0–1521	0.160	0.160	0.160
1521–3558	0.160	0.160	0.160
3558–5900	0.145	0.145	0.145
5900–6672	0.137	0.137	0.137
6672–7050	0.124	0.110	0.137

The wellbore pressure is calculated under the three schemes using the model described in Section 2.3.1, as depicted in Figure 10. Scheme 1 and scheme 2 were found to fall within the safe density window range. However, in scheme 3, the equivalent cycle density (ECD) in the section 6800–7050 m exceeded the ECD of the leakage layer. Running the casing at a low speed can lead to a slower construction progress and increased nonproductive time, thereby raising the overall well budget. Consequently, the casing speed of scheme 1 is selected for the operation.

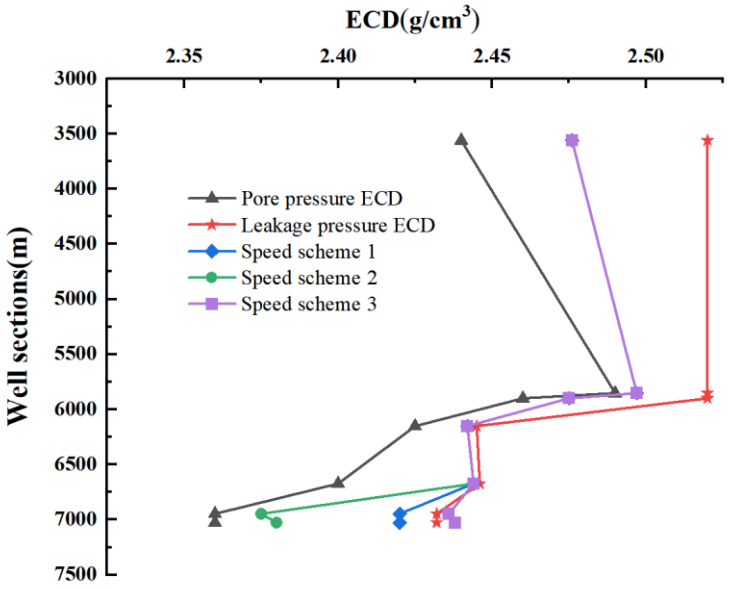

Figure 10. ECD changes of different casing running speed schemes.

Based on the calculation model for surge pressure and wellbore pressure, the surge pressure generated at each casing speed in scheme 1 and the corresponding annular back pressure required during casing running can be determined, as presented in Table 6.

Table 6. The surge pressure, casing running speed and back pressure.

Casing into the Well Section (m)	Surge Pressure (MPa)	Casing Speed (m/s)	Back Pressure (MPa)
0–1523	0.32	0.160	—
1523–3560	0.77	0.160	1.641
3560–5900	1.74	0.145	3.427
5900–6672	1.70	0.137	4.041
6672–7050	1.80	0.124	4.457

The calculation results from Tables 4 and 6 were successfully applied during the casing running operation of Well LT-X1, resulting in a smooth operation without any well leakage or overflow.

4. Discussion

The model studied in this paper still has limitations and uncertainties, which include:

(1) Insufficient validation in practical applications: Although managed-pressure casing running technology under NPWs was developed for Well LT-X1, further validation is required to assess its applicability to other wells and different geological conditions.
(2) Model accuracy and assumptions: The models established in the study may be based on certain assumptions and simplifications, which can impact the accuracy and applicability of the models. Therefore, when using these models for wellbore pressure calculations, it is important to evaluate the accuracy of the models and the assumptions they rely on and make adjustment or corrections as necessary.
(3) Data availability and parameter selection: The accuracy and reliability of wellbore pressure calculation models are limited by the availability of data. In practical applications, there may be instances of missing or incomplete data, which can affect the accuracy of the calculated results. Additionally, the selection and estimation of parameters involved in the models can also impact the results, requiring careful consideration and reasonable estimation.

In conclusion, although the study achieved certain results under specific conditions, further research and practice are needed to overcome these limitations.

5. Conclusions

This paper, using Well LT-X1 as an example, simulated the casing running process and the changes in the slurry column structure of drilling fluids. A circulation scheme is designed as follows: Circulate 125 m^3 of drilling fluid with a density of 2.45 g/cm^3 and 155 m^3 of drilling fluid with a density of 2.35 g/cm^3 at a depth of 3560 m. From there, circulate 164 m^3 of drilling fluid with a density of 2.35 g/cm^3 at a depth of 5900 m. Finally, at a depth of 7050 m, circulate 250 m^3 of drilling fluid with a density of 2.30 g/cm^3. The casing running speeds and back-pressure values were designed as follows for the respective well sections: 0–1523 m: 0.160 m/s casing speed, 0MPa back pressure; 1523–3560 m: 0.160 m/s casing speed, 1.641 MPa back pressure; 3560–5900 m: 0.145 m/s casing speed, 2.427 MPa back pressure; 5900–6674 m: 0.137 m/s casing speed, 4.041 MPa back pressure; 6674–7050 m: 0.124 m/s casing speed, 4.457 MPa back pressure. The results demonstrate that by optimizing the structure of multi-density gradient drilling fluid and applying annular back pressure in stages, along with the accurate calculation of wellbore pressure, the goals of leak-proofing and pressure stabilization can be achieved.

This study provides a foundation for managed-pressure running casing technology under NPWs. The established model for wellbore slurry column structures and wellbore pressure calculations under managed-pressure running casing serves as a theoretical basis for casing running technology under NPWs.

Author Contributions: Investigation, M.J.; Resources, Z.Z.; Writing—original draft, Y.M.; Writing—review & editing, H.Y. All authors have read and agreed to the published version of the manuscript.

Funding: This research was funded by Engineering Technology Research Institute of PetroChina West Drilling Engineering grant number xzgcy2021-055.

Institutional Review Board Statement: Not applicable.

Informed Consent Statement: Not applicable.

Data Availability Statement: Data is unavailable due to privacy or ethical restrictions.

Acknowledgments: The authors wish to express their appreciation to the Engineering Technology Department of Western Drilling Company for their assistance with the experimental study and kindly supplying data.

Conflicts of Interest: The authors declare no conflict of interest.

References

1. Wang, F.; Liu, X.; Jiang, B.; Zhuo, H.; Chen, W.; Chen, Y.; Li, X. Low-loading Pt nanoparticles combined with the atomically dispersed FeN_4 sites supported by Fe_{SA}-N-C for improved activity and stability towards oxygen reduction reaction/hydrogen evolution reaction in acid and alkaline media. *J. Colloid Interface Sci.* **2023**, *635*, 514–523. [CrossRef] [PubMed]
2. Li, Q.; Zhang, C.; Yang, Y.; Ansari, U.; Han, Y.; Li, X.; Cheng, Y. Preliminary experimental investigation on long-term fracture conductivity for evaluating the feasibility and efficiency of fracturing operation in offshore hydrate-bearing sediments. *Ocean. Eng.* **2023**, *281*, 114949. [CrossRef]
3. Li, Q.; Zhao, D.; Yin, J.; Zhou, X.; Li, Y.; Chi, P.; Han, Y.; Ansari, U.; Cheng, Y. Sediment instability caused by gas production from hydrate-bearing sediment in Northern South China Sea by horizontal wellbore: Evolution and mechanism. *Nat. Resour. Res.* **2023**, *32*, 1595–1620. [CrossRef]
4. Kudźma, Z.; Stosiak, M. Reduction of infrasounds in machines with hydrostatic drive. *Acta Bioeng. Biomech.* **2013**, *15*, 51–64. [CrossRef] [PubMed]
5. Clark, E.H. A graphic view of pressure surges and lost circulation. In *Drilling and Production Practices*; American Petroleum Institute: New York, NY, USA, 1956.
6. Moore, P.L. Pressure surges and their effect on hole conditions. *Oil Gas J.* **1965**, *63*, 90.
7. Clark, R.K.; Fontenot, J.E. Field measurements of the effects of drillstring velocity, pump speed, and lost circulation material on downhole pressures. In Proceedings of the Fall Meeting of the Society of Petroleum Engineers of AIME, Houston, TX, USA, 6–9 October 1974; SPE Annual Technical Conference and Exhibition. Society of Petroleum Engineers (SPE): Richardson, TX, USA, 1974. [CrossRef]
8. Lal, M. Surge and swab modeling for dynamic pressures and safe trip velocities. In Proceedings of the IADC/SPE Drilling Conference, New Orleans, LA, USA, 20–23 February 1983; Society of Petroleum Engineers (SPE): Richardson, TX, USA, 1983.
9. Wagner, R.R.; Halal, A.S.; Goodman, M.A. Surge field tests highlight dynamic fluid response. In Proceedings of the SPE/IADC Drilling Conference, Amsterdam, The Netherlands, 22–25 February 1993; Society of Petroleum Engineers (SPE): Richardson, TX, USA, 1993. [CrossRef]
10. Bing, Z.; Kaiji, Z.; Qiji, Y. Equations help calculate surge and swab pressures in inclined wells. *Oil Gas J.* **1995**, *93*, 38.
11. White, W.W.; Zamora, M.; Svoboda, C.F. Downhole measurements of synthetic-based drilling fluid in offshore well quantify dynamic pressure and temperature distributions. *SPE Drill. Complet.* **1997**, *12*, 149–157. [CrossRef]
12. Ward, C.; Andreassen, E. Pressure-while-drilling data improve reservoir drilling performance. *SPE Drill. Complet.* **1998**, *13*, 19–24. [CrossRef]
13. Rudolf, R.L.; Suryanarayana, P.V.R. Field Validation of Swab Effects While Tripping-In the Hole on Deep, High Temperature Wells. In Proceedings of the SPE/IADC Drilling Conference, Dallas, TX, USA, 3–6 March 1998; Society of Petroleum Engineers (SPE): Richardson, TX, USA, 1998. [CrossRef]
14. Isambourg, P.; Bertin, D.L.; Brangetto, M. Field hydraulic tests improve HPHT drilling safety and performance. *SPE Drill. Complet.* **1999**, *14*, 219–227. [CrossRef]
15. Samuel Robello, G.; Sunthankar, A.; McColpin, G.; Bern, P.; Flynn, T. Field validation of transient swab/surge response with PWD data. In Proceedings of the SPE/IADC Drilling Conference, Amsterdam, The Netherlands, 27 February–1 March 2001; Society of Petroleum Engineers (SPE): Richardson, TX, USA, 2001. [CrossRef]
16. Rommetveit, R.; Bjørkevoll, K.S.; Gravdal, J.E.; Goncalves, C.J.C.; Lage, A.C.V.M.; Campos, J.E.A.; Aragão, Á.F.L.; Arcelloni, A.; Ohara, S. Ultradeepwater hydraulics and well-control tests with extensive instrumentation: Field tests and data analysis. *SPE Drill. Complet.* **2005**, *20*, 251–257. [CrossRef]
17. Cannon, G.E. Changes in Hvdrostatic Pressure Due to Withdrawing Drill Pipe from the Hole. In *Drilling and Production Practices*; American Petroleum Institute: New York, NY, USA, 1934.
18. Ormsby, G.S. Calculation and Control of Mud Presures in Drilling and Completion Operations. In *Drilling and Production Practices*; American Petroleum Institute: New York, NY, USA, 1954.
19. Clark, E.H. Bottom-hole pressure surges while running pipe. *Pet. Eng. Int.* **1955**, *27*, B68.
20. Burkhardt, J.A. Wellbore pressure surges produced by pipe movement. *J. Pet. Technol.* **1961**, *13*, 595–605. [CrossRef]
21. Schuh, F.J. Computer makes surge-pressure calculations useful. *Oil Gas J.* **1964**, *31*, 96.
22. Fontenot, J.E.; Clark, R.K. An improved method for calculating swab and surge pressures and circulating pressures in a drilling well. *Soc. Pet. Eng. J.* **1974**, *14*, 451–462. [CrossRef]
23. Haige, W.; Xisheng, L. Study on steady surge pressure for yield-pseudoplastic fluid in a concentric annulus. *Appl. Math. Mech.* **1996**, *17*, 15–23. [CrossRef]
24. Jinchang, W. Analysis of annular fluctuation pressure pattern during casing running operation in Da-niudi Gas Field. *Oil Drill. Prod. Technol.* **2016**, *38*, 36–41. [CrossRef]
25. He, S.; Srivastav, R.; Tang, M.; Ahmed, R. A new simplified surge and swab pressure model for yield-power-law drilling fluids. *J. Nat. Gas Sci. Eng.* **2016**, *28*, 184–192. [CrossRef]
26. Lubinski, A.; Hsu, F.H.; Nolte, K.G. Transient pressure surges due to pipe movement in an oil well. *Rev. Inst. Fr. Pét.* **1977**, *32*, 307–348. [CrossRef]
27. Zhong, B.; Zhou, K.J.; Yuan, Q.J. Equations help calculate surge and swab pressures in inclined well. *Oil Gas J.* **1995**, *18*, 74–77.

28. Zhang, F.; Kang, Y.; Wang, Z.; Miska, S.; Yu, M.; Zamanipour, Z. Real-time wellbore stability evaluation for deepwater drilling during tripping. In Proceedings of the SPE Deepwater Drilling and Completions Conference, Galveston, TX, USA, 14–15 September 2016; Society of Petroleum Engineers (SPE): Richardson, TX, USA, 2016.
29. Pengcheng, W.; Chaoyang, X.; Yingfeng, M.; Hongtao, L. Laws fo bottomhole transient pressure fluctuation during tripping in narrow safety density window formation. *Drill. Prod. Technol.* **2016**, *39*, 22–25.
30. Dong, T. Study on Drilling Overflow Monitoring Method and Application for Pressure-Sensitive Formation. Master's Thesis, Southwest Petroleum University, Chengdu, China, 2018.
31. Junbo, Q. Research on Calculation of Surge and Swab Pressures and Control of Gas Kick in Constant Bottom Hole Managed Pressure Drilling. Ph.D. Thesis, Northeast Petroleum University, Daqing, China, 2019.
32. Karpenko, M. Landing gear failures connected with high-pressure hoses and analysis of trends in aircraft technical problems. *Aviation* **2022**, *26*, 145–152. [CrossRef]